Analysis of Formation of an Individual Droplet using a High-Resolution Multi-Exposure Imaging System

Ingo Reinhold,[1,2] Karsten Sitterberg,[1] Matthias Müller,[1] Mamat Abdulla,[3] Sergei Popov,[3] Wolfgang Voit,[1] Werner Zapka[1,2]; [1] XaarJet AB, Järfälla, Sweden; [2] KTH Royal Institute of Technology, iPack Vinn Excellence Center, Stockholm, Sweden; [3] KTH Royal Institute of Technology, Department of Materials and Nano-physics, Stockholm, Sweden

Abstract

Localized dispensing of precious functional materials has attracted considerable interest in the academic as well as the industrial society. While the number of publications show numerous fields of applications in printed electronics, photovoltaics, display technologies and thin functional coatings, the transition into the industrial sector is often hindered by challenges resulting from ink-printhead combinations and their implications on reliability and stability of the process, as well as side-effects such as mist accumulation in heavy duty printing equipment.

While measuring equipment to quantify various rheological and interfacial parameters for fluid optimization has been developed with the accompanying mathematical models, the physical jetting experiment as well as high-duty printing trials cannot yet be substituted by these methods. In order to quantify the generation of a droplet alongside with its tailing behavior and mist formation as well as statistics based on cross-talk effects and relaxation-related effects, high-resolution and high-speed imaging are required.

This paper examines the optical setup and outlines the required calculations for establishing sharp, high-resolution images using a combination of a high power laser diode with a resonant MEMS micro mirror with a theoretical resolution of 1.8 µm. The limitations of the setup regarding the achievable resolution as well as potential improvements are assessed. Furthermore, the experimental setup, including repetitive generation of nanosecond-pulses necessary for motion-blur-free images, will be discussed. Additionally, results from imaging a droplet formation process using a Xaar 126 printhead are discussed.

Introduction

Functional printing applications have triggered a variety of research towards a more fundamental understanding of the printing process[1]. Specifically for inkjet printing applications the understanding of the complex relationship between rheological and interfacial effects at different shear-rates, interfacial stress states as well as the driving frequencies has been broadened by new mathematical models and simulation tools that aid the efficient development of fluids for low satellite count and high reliability [2].

The analysis of jetting as a predictor for the performance of a fluid-printhead combination has been reported in miscellaneous publications and has been introduced for commercial applications by various suppliers [3,4]. While affordable solutions typically use stroboscopic illumination in order to achieve some understanding of the droplet formation process and its stability, these systems are typically not capable of capturing the droplet formation event of a single droplet over the course of time. High-speed cameras on the contrary are available with temporal resolutions of Megaframes per second, but are limited in the achievable image resolution at their maximum frame rates.

In this paper we present a novel approach to combine the stroboscopic illumination with the approach of high-speed imaging. The pulse train of a triggered laser illuminates the droplet being formed at the nozzle. Using the slow and fast axis of the diode to illuminate a rectangular field, this beam is suited to image a drop from the nozzle up to a distance of 2 mm along its trajectory. The beam from the laser diode is then magnified using an optical setup and swept over the CCD-chip of a low-speed camera using a resonant MEMS-mirror device, placing images in the course of time next to each other on the sensor array. In this fashion up to 10 high-resolution images of the same droplet can be captured during its transition from the nozzle plate to a typical throw distance of 1-1.5 mm.

System design

A schematic design of the system under consideration is presented in Figure 1. The system comprises three essential parts: (1) the imaging part, (2) an alignment part to cope with the resonant oscillation of the mirror and (3) a controller part to synchronize the illumination, droplet ejection, the mirror motion as well as the image acquisition.

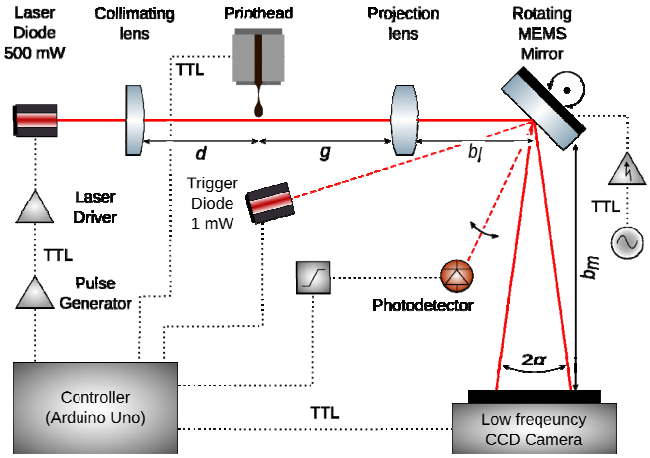

Figure 1: Schematic overview of the system including the illumination and triggering system [full lines: laser beam path, dashed lines: alignment laser beam path, dotted lines: electrical signal paths].

Laser considerations

The different apertures experienced by the laser radiation upon exit from the diode create an elliptical beam profile based on the divergence angles θ in direction of the width and the height of the output area of the semiconductor. While this characteristic may be unwanted in some applications, here we make use of this fast-slow axis behavior in order to illuminate the vicinity of the droplet with a minimum loss of photons. For this reason, collimation can be accomplished using a single cylindrical length with a focal length f_c and a numerical aperture NA of the incident beam equivalent to $sin(\theta/2)$, which will create a diameter d_b in the fast axis of

$$d_\mathrm{b} = 2 f_\mathrm{c} \mathrm{NA}$$

which results in a strong beam broadening in the fast axis and minor widening in the slow axis creating a line profile.

Illumination conditions

To omit motion blur, the object under consideration may not move more than one tenth of its characteristic size [5] during the illumination time t_{ill}. Considering droplet formation at a velocity v lower than 10 ms^{-1} and sizes larger than 5 µm this requires an illumination time smaller than 50 ns.

The required amount of photons during an illumination period can be estimated from the desired signal-to-noise ratio (SNR), which can be calculated using

$$\mathrm{SNR} = \frac{S_\mathrm{ph}}{\sqrt{\delta_\mathrm{ph}^2 + \delta_\mathrm{d}^2 + \delta_r^2}}$$

where S_ph represents the incident photon signal and δ are the photon noise *(ph)*, dark noise *(d)* and the read-out noise *(r)*, respectively.

The photon noise results from the quantum nature of photons, which follows a Poisson distribution and has a fluctuation equal to the square root of the incoming photon signal. This signal can be calculated using $I\, t_\mathrm{ill} Q_\mathrm{e}$, where I is the incident photon flux and Q_e is the quantum efficiency of the used sensor. The photon noise therefore results in

$$\delta_\mathrm{ph} = \sqrt{S_\mathrm{ph}} = \sqrt{I\, t_\mathrm{ill} Q_\mathrm{e}}$$

The dark current noise, originating from thermal fluctuations in the sensor, introduces a noise as the integral of the dark current I_d over the exposure time t_{exp}. Assuming a Poisson distributed effect this gives

$$\delta_\mathrm{d} = \sqrt{I_\mathrm{d} t_\mathrm{exp}}$$

Finally, the read-out noise δ_r is related to the amplifier circuit of the sensor and therefore specific for the system used.

Recalling that the number of photons N is equal to $I t_\mathrm{ill}$ one can rearrange the equation to the desired number of photon. For simplification we assume the exposure time will be reasonably short and therefore, dark current noise will be nil. The number of required photons per pixel can then be calculated using

$$N \approx \frac{\mathrm{SNR}^2}{2Q_e}\left(1 + \sqrt{1 + \frac{4\delta_\mathrm{r}^2}{\mathrm{SNR}^2}}\right)$$

In order to allow for a comparison to the number of photons provided by the laser, one can calculate the emitted number by comparing the energy of the laser E_{las} and the illumination time t_{ill} with the energy of a photon E_{ph}, giving

$$n_\mathrm{las} = \frac{E_\mathrm{las}}{E_\mathrm{ph}} = \frac{P_\mathrm{las} t_\mathrm{ill} \lambda}{hc}$$

where P_{las} is the nominal power of the laser, λ is the wavelength of the radiation, h is the Planck constant and c is the speed of light.

This number of photons will be distributed over the amount of pixels illuminated by a single laser pulse. As the maximum usable pixel area of the CCD sensor is 1280×960 px^2, with a physical dimension of 4.8×3.6 mm^2 [6], a division into 10 slices results into exposure areas of 128×960 px^2, or 480×3600 μm^2.

The calculation given above results in 123840 illuminated pixels. Using a desired SNR of 20 [7] for good contour reproduction, Q_e of 0.5 at a wavelength λ of 630 nm and an assumed read-out noise of δ_r of 10 e^- the desired number of photons per pixel equates to 970 and for the complete strip 1.2×10^8 photons. Using the calculated illumination time of 50 ns, a peak power of the laser of 600 mW and the speed of light in vacuum, the total number of photons leaving the laser results to 9.7×10^{10}. This results in a ratio of emitted to required photons of 815, which leaves a margin of almost three orders of magnitude.

Projection optics

In order to have a sharp projection with a fixed magnification simple calculations using the Gaussian lens were used. Assuming no distortion effects from the MEMS mirror, the image distance is simply a sum of the distance b_L from lens to the mirror and b_M from the mirror to the CCD surface. Taking into account a magnification of two and a focal length f of the lens being 75 mm, the object distance equates to 112.5 mm and the image distance to 225 mm.

Theoretical resolution

The minimum optically resolvable feature size $d_{min,opt}$ is determined by [8]

$$d_\mathrm{min,opt} = 1.22\lambda\frac{g}{L}$$

where g is the object distance and L is the diameter of the lens used. With the numbers given in the previous section this equates to a minimum feature size of 1.8 µm.

When resolving this feature with a digital sensor, the Nyquist-Shannon sampling theorem can be rewritten to give, with consideration of the magnification M of the system and the available pixel size d_p, the digitally resolvable feature size $d_{min,dig}$ as

$$d_\mathrm{min,dig} = \frac{2d_p}{M}$$

For the given sensor and a magnification of two, this restricts the resolution of the system to the pixel size of 3.75 µm.

The pixel size furthermore relates to the depth of focus that can be achieved. In order to calculate the depth of focus δ_f one can consider the lens diameter L, the pixel size d_p and imaging distance b and yield

$$\delta_\mathrm{f} = \frac{2d_\mathrm{p} b}{L}$$

This gives for the given values a depth of focus of 33.8 µm.

Implications of the resonant MEMS mirror

Resonant MEMS mirrors provide a constant tilting frequency and an amplitude, which can be modulated using the sinusoidal driving signal.

The required tilting angle of the mirror α_m, can be calculated using

$$\alpha_m = \tan^{-1}\left(\frac{w_s}{2b_m}\right)$$

where w_s is the width of the sensor and b_m is the distance between the mirror and the sensor. For the given sensor and b_m being 100 mm this yields 1.37°. A typical transit of a droplet with a velocity 10 ms^{-1} and a throw distance of 1mm gives a total transit time of 100 µs, which dictates the resonating frequency of the mirror to 5 kHz and, assuming linear motion, the velocity of the beam on the CCD sensor to be 48 ms^{-1}. Recalling the criterion for motion-blur-free images and keeping 50 ns as illumination time, the system is limited to a spherical feature of 6.9 pL in volume.

The tilting of the mirror also introduces a change in the imaging distance as the beam path increases. The change in path length can be estimated using the Pythagorean theorem and yield

$$\Delta = \sqrt{\left(\frac{w_s}{2}\right)^2 + b_m^2} - b_m$$

A comparison with the depth of focus found above indicates that a b_m of 100 mm yield sufficiently low distortion with 29 µm. At 50 mm imaging distance the change in path length yields 58 µm, respectively, and will therefore reduce the image quality by blurring images at the maximum deflection of the mirror. This, however, is only true if the aperture posed by the mirror is not considered. Recalling the equation given above and replacing the aperture of the lens with the diameter of the mirror and the imaging distance with b_m equal to 50 mm changes the depth of focus to 125 µm, which reliefs the constraints on the distance between mirror and sensor.

Experimental

The system as depicted in Figure 1 has been realized on an optical breadboard table, using a 500mW, 638 nm laser diode (ML520G72, peak power 600 mW, Mitsubishi Electric, JP) with an appropriate collimation lens (focal length 3.1 mm, 352330-A, Thorlabs, UK). Driving the laser diode was accomplished using a commercially available laser driver module (iC-HG HG1D, iC-Haus, DE). Imaging was carried out with a projection lens having a focal length of 75 mm and a diameter of 50 mm. The projection was swept over a progressive CCD sensor (Pixel size 3.75x3.75 μm^2, ICX445, Sony, JP) using an off the shelf VarioScan MEMS mirror (diameter 3 mm, tilt angle 8°, Fraunhofer IPMS, DE) with a resonant frequency of 5.85 kHz and a diameter of 3 mm. The mirror was driven at twice its resonance frequency using a sinusoidal signal from a function generator (Model 164, Wavetek, US) amplified by a high voltage converter (WMA-01, Falco Systems, NL).

The system was controlled using an Arduino UNO (Arduino, IT). To generate short pulses from the output of the micro controller a monostable multi-vibrator (DM74123, Fairchild, US) was connected to a resistor of 5 kΩ and a capacitance of 1 pF. The triggering setup comprised a 1 mW red laser pointer and a photodetector (AEPX65, Centronic, UK) supplied with a 5V bias voltage. Waveforms were recorded with a digital oscilloscope (PicoScope 2206B, Pico Technology, UK).

Jetting experiments were carried out using a Xaar 126/50 pL printhead with an unpigmented oil ink (Toyo Ink Group, JP) at room temperature. The waveform was chosen such that the droplet velocity yielded 6 m/s.

Results and Discussion

Triggering Signals

In order to extract signals with sufficient amplitude for triggering the interrupts of the Arduino microcontroller, a 1 MΩ resistor was connected in series with the photodetector. The resulting amplitude response of the MEMS mirror as a function of driving voltage to the mirror and hence tilting angle is show in Figure 2.

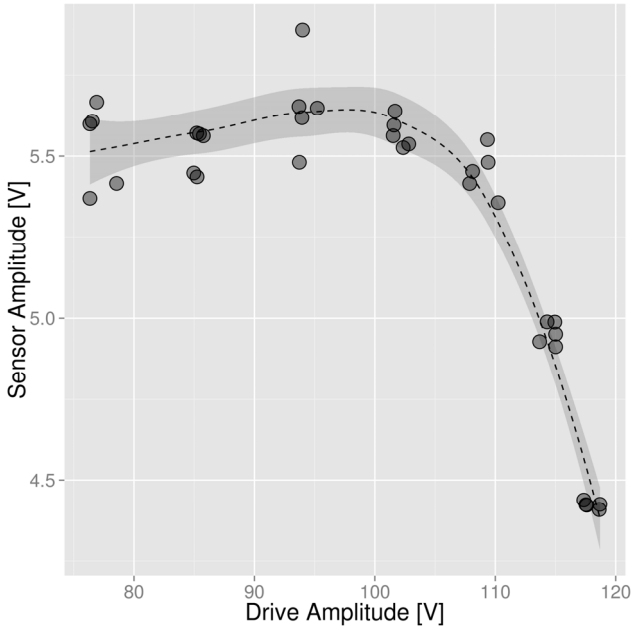

Figure 2: Triggering signal amplitude as a function of excitation amplitude, i.e. mirror deflection, measured using a 1 MΩ sensing resistor.

The response clearly indicated a stable condition of the signal for driving voltages up to 110 $V_{p\text{-}p}$. Above this level the amplitude of the oscillation was too high and hence the speed of the reflected laser beam and the resulting short interaction time with the diode was insufficient to generate the required voltage level. According to the specification, a peak-to-peak voltage of 110 V generates deflection amplitudes of 5.5° and thereby renders the detection circuit adequate for the desired application.

The location of the triggering diode in the produced light fan can furthermore improve the robustness of the system. Figure 3 shows the resulting triggering signal for varying diode positions relative to the center of the trajectory of the sensing beam. The duty cycle of the triggering pulses changed as the distance to inflection changed. This made it difficult to select the correct mirror direction for imaging. Therefore, the maximum

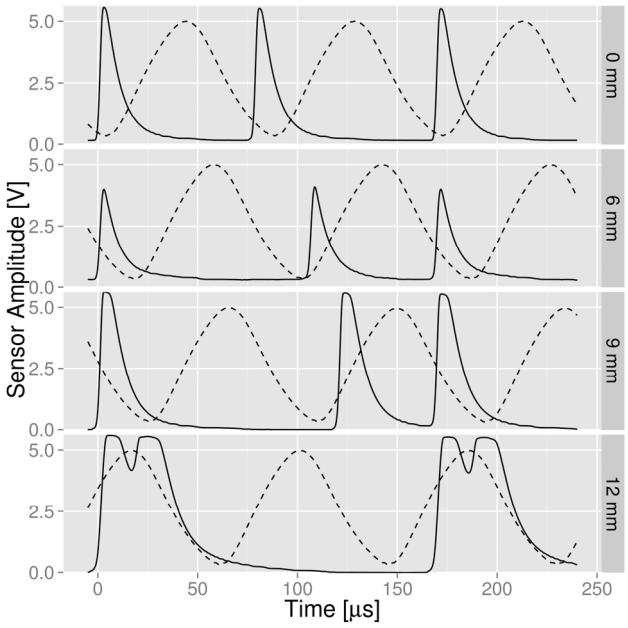

Figure 3: Influence of the photodetector position in the trajectory of the sensing laser on the dwell time and the duty cycle of recurring trigger impulses [solid line: photodetector signal, dashed line: normalized agitation signal of the mirror]

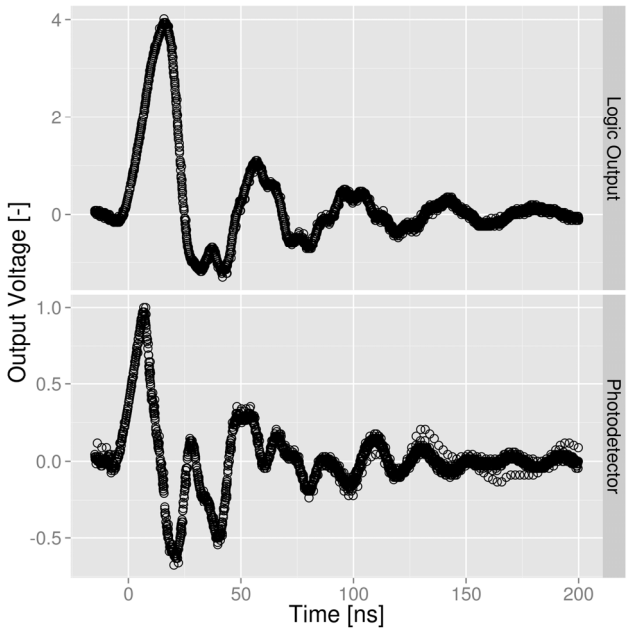

Figure 4: Outputs from the pulse generation unit and the resulting laser output measured using a AEPX65 photodetector over a 1MΩ resistor and normalized to its maximum value.

displacement of 12 mm was chosen to position the triggering sensor so that the error introduced by left- and right going mirror movements was minimized.

Pulse generation

As was discussed in the design section, a very short, high intensity light flash from the laser diode was desirable in order to achieve motion-blur-free images with a good signal to noise ratio. In order to produce these signals using the outputs of a Arduino microcontroller, an intermediate pulse-shortening logic had to be implemented, converting the >5 µs long pulses from the controller.

A monostable multi-vibrator in conjunction with a variable resistor being set to 5 kΩ and a 1 pF capacitance produced stable single pulses upon experiencing the rising edge coming from the microcontroller. Figure 4 shows the superposition of 30 successively recorded pulses from the shortening logic and confirms the pulse width reduction to a FWHM of 13.5 ± 0.2 ns and a characteristic pulse length (e^{-4} level) of 32.6 ± 0.5 ns. While the first pulse was clearly visible, some remaining oscillation was detected which we attributed to interactions of the externally connected capacitance as well as the input impedance to the oscilloscope. The observed fluctuations, however, did not exceed the 2 V triggering threshold voltage of the laser driver and was therefore neglected.

In order to quantify the light output from the laser diode when using the triggering signal provided by the pulse shortening logic, a photodiode with a risetime of 0.6 ns was wired to a sensing resistor. The normalized results are depicted in Figure 4. Using a Gaussian fit for the pulse, a FWHM of 9.0 ± 0.2 ns and a characteristic width of 21.7 ± 0.5 ns were found. Here the sensing resistor in conjunction with the input impedance of the measurement equipment cause the current to lower the bias of the diode and generate a negative flowing current, which then resonates in the system.

The obtained results proved the illumination capbility of the system to provide light pulses much shorter than 50 ns. The photon dose was accordingly adjusted using the incorporated variable resistor as well as the diode current in order to give high contrast images.

Jetting

In order to demonstrate the capabilities of the system a Xaar 126/50 pL printhead was mounted and operated at room temperature. The triggering circuit was connected to the external electronics of the printhead, which allowed for defined firing and setting of a time delay.

Figure 5 depicts the droplet formation of a single droplet using the described multi-exposure system. In this depiction the sinusoidal characteristic as superimposed by the motion of the mirror was removed digitally to give a better impression of the drop formation process. The image sequence shows ejection of a droplet with a long filament as a result of the break-up between the fluid in the nozzle and the forward accelerated fluid mass (1). Already at this stage a non-axisymmetric tail geometry was observed, which moved over the length of the tail with time (1-3). The instability finally triggered the disintegration of the long filament (4-6), leaving the main droplet connected to a first satellite by a very thin thread (6). In the course of time surface tension formed round droplets (7) and merged succeeding satellites into a larger one, which traveled at a similar velocity as the main droplet.

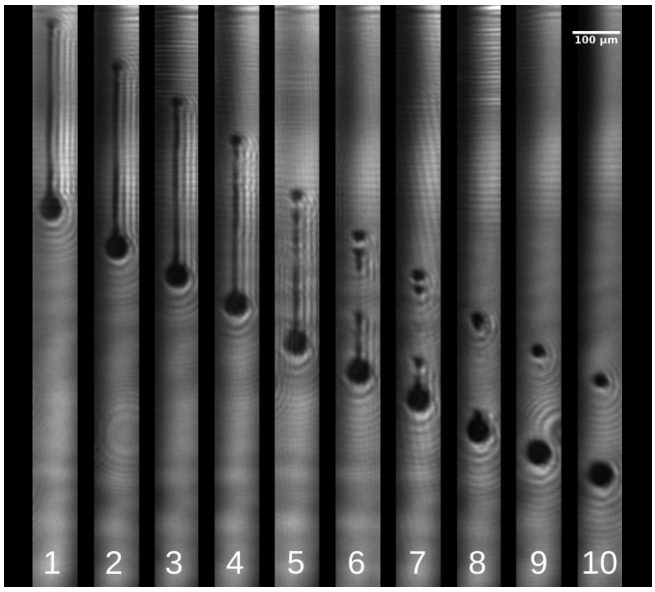

Figure 5: Recorded droplet formation from a Xaar 126 50 pL printhead as recorded with the described system. The sinusoidal distribution of the exposures has been removed by software for better visibility. [Analogue ink, $v_{droplet}$ 6 m/s, Δt 10 µs, VHDL voltage 3.4 V, $V_{mirror,p\text{-}p}$ 110 V]

The quality of the image appeared reasonable to resolve rather fine features as the thin filamentary connection of the main droplet and the first satellite (cf. Figure 5 exposure 6). However, the overall impression did not resemble the theoretical resolution. Multiple influences can be considered for the reduction of the theoretical limit.

The reduced apparent resolution of the images can be explained by various effects. Being limited by the cell size the resolution of the sensor in combination with the magnification of the optical setup, the minimum resolvable feature equates to 3.75 µm. A larger influence in the presented system is the motion blur, which results from the velocity of the light beam sweeping over the sensor. The limit of resolution is reduced to features of 13.8 µm using the criterion for motion blur and an illumination time of 28 ns. This represents an uncertainty range of roughly four pixels and accounts for the blurriness in our images. A possible relief for this is the reduction of the pulse width alongside with an increase in the current through the diode to trigger higher photon emission. Alternatively, reducing the sweeping angle of the mirror, less exposures and smaller sensors could be used to reduce the sweeping amplitude of the light beam and therefore its velocity. Another reduction in resolution could originate from the small aperture of the MEMS mirror.

The homogeneity of the laser diode output did vary rather strongly over the longitudinal direction of the laser and, therefore, inhibits the generation of a constant contrast. Additional means such as background subtraction or camera internal look-up-tables could be considered to relieve the effects, while diffusor plates typically absorb too much of the radiation to enable a suitable signal-to-noise ratio.

The imaging depicted in Figure 5 furthermore showed some interference patterns, originating from the diffraction of the monochromatic radiation by the shape of the droplets but also from debris in the beam path. For a visual inspection of the images, these do not pose a major obstacle, but will for the numerical analysis using thresholding techniques. Means for reducing these effects have been widely discussed in the literature [9,10] and are fully applicable to the system.

Conclusion and Outlook

The results presented in this paper confirm the principal applicability of a MEMS mirror device for the projection of a single droplet formation process onto a high resolution sensor. By estimating the necessary photon emission from a high power laser diode and designing an optical setup for sharp imaging of fast objects a first proof-of-principle design could be established and delivered reproducible results. A pulse shortening circuit was implemented and showed good performance in reducing the pulse width from an Arduino driver with pulse lengths > 5 µs to pulses shorter than 40 ns at the e^{-4} level.

The physical setup including a 5.85 kHz MEMS micro mirror was able to reproducibly record droplet formation processes. The achievable image quality, however, did not resemble the theoretical resolution of the optical setup. The deterioration was attributed to the motion blur induced by the fast scanning of the light beam across the sensor, the resolution of the sensor chip as well as the additional aperture introduced by the mirror.

Further steps will include optimization of the light homogeneity of the laser, optimization of the mirror-sensor combination as well as suitable post-processing techniques for the acquired images.

References

[1] Basaran, O. a., Gao, H., & Bhat, P. P. (2013). Nonstandard Inkjets. Annual Review of Fluid Mechanics, 45(1), 85–113.
[2] Morrison, N. F., & Harlen, O. G. (2010). Viscoelasticity in inkjet printing. Rheologica Acta, 49(6), 619–632.
[3] www.imagexpert.com, last accessed Jun 2013.
[4] www.oxfordlasers.com/imaging/, last accessed Jun 2013.
[5] A. Whybrew, “High-Speed Imaging”, Oxford Lasers Technical Report, 2002.
[6] Guppy Pro F-125, Technical Manual, Allied Vision Technologies, 2011.
[7] Sabharwal, Y. Digital Camera Technologies for Scientific Bio-Imaging. Part 4: Signal-to-Noise Ratio and Image Comparison of Cameras. Microscopy and Analysis, 26(1), 2012.
[8] Peter W. Milonni and Joseph H. Eberly. Laser Physics. John Wiley & Sons, Inc., 2010.
[9] A. van der Bos, Air entrapment and droplet formation in inkjet printing, PhD thesis, TU Twente, NL, 2010.
[10] S. D. Hoath, G. D. Martin, J. R. Castrejón-Pita, and I. M. Hutchings, Satellite formation in drop-on-demand printing of polymer solutions”, Proc. IS&T’s NIP23 (IS&T, Springfield, VA, 2007) pp. 331–335.

Author Biography

Ingo Reinhold graduated in micromechanics-mechatronics with emphasis on print- and media technology from Chemnitz University of Technology in 2008. After joining Xaar’s Advanced Application Technology group in Järfälla, Sweden, he focused on advanced acoustic driving of piezo-type inkjet printheads alongside with pre- and post-processing of functional materials in digital fabrication. He is currently enrolled as a PhD student within the iPack VINN Excellence Center at the Royal Institute of Technology (KTH) in Stockholm, Sweden.